Journal of Sound and Vibration (1998) **212**(2), 321–336

EXPERIMENTAL AND NUMERICAL ANALYSIS OF THE STEADY STATE BEHAVIOUR OF A BEAM SYSTEM WITH IMPACT

E. L. B. VAN DE VORST

Department of Mechanical Engineering, Eindhoven University of Technology, P.O. Box 513, 5600 *MB, Eindhoven, The Netherlands and TNO Centre for Mechanical Engineering, P.O. Box* 49, 2600 *AA, Delft, The Netherlands*

M. F. HEERTJES, D. H. VAN CAMPEN and A. DE KRAKER

Department of Mechanical Engineering, Eindhoven University of Technology, P.O. Box 513, 5600 *MB, Eindhoven, The Netherlands*

AND

R. H. B. FEY

TNO Centre for Mechanical Engineering, P.O. Box 49, 2600 *AA, Delft, The Netherlands*

(*Received* 17 *April* 1997, *and in final form* 1 *December* 1997)

In this paper the steady state behaviour of a beam system with a periodically moving support and an elastic stop is analysed both numerically and experimentally. In the numerical analysis a continuous model for the elastic stop is used based on the contact force law of Hertz. The beam is modelled using finite elements and subsequently reduced using a component mode synthesis method leading to a non-linear six-degree-of-freedom model. The steady state behaviour of this model is investigated by calculating periodic solutions while varying the excitation frequency. This is done by solving two-point boundary value problems using the multiple shooting method in combination with a path-following method. Experimental research concerning periodic solutions is carried out to verify the numerical results. The experimental results correspond very well with the numerical results. It appears that the high eigenfrequencies of the linear beam system strongly influence the low-frequency non-linear steady state response. This means that multi-degree-of-freedom models are important for an accurate representation of the actual system behaviour, although a single-degree-of-freedom model captures important first-order information about a lot of the non-linear phenomena in the low-frequency range.

1. INTRODUCTION

In many practical engineering applications of mechanical systems, impacts at stops occur. It is important to carry out a dynamical analysis of such systems, to identify and subsequently reduce the noise and wear caused by repeated unacceptably large impacts. Examples of such systems are gear rattle, heat exchanger tube wear in nuclear power stations and ships colliding against fenders. Systems with stops are typical examples of systems with local non-linearities. Although the non-linearity is local, the overall dynamic response of the system in general changes drastically. A system with stops cannot be linearized, so it is very difficult to predict the system response without a non-linear analysis.

In recent years, non-linear dynamical systems have been studied by many researchers. For a general introduction to non-linear dynamics the reader is referred to Guckenheimer

0022–460X/98/170321 + 16 $25.00/0/sv971447

and Holmes [1], Thompson and Stewart [2], Parker and Chua [3] and Thompson [4]. The long term behaviour of a non-linear system, which is excited by a periodic external load, can be periodic, quasi-periodic, or chaotic. The period of a periodic attractor may be equal to the excitation period (harmonic), but may also be a multiple of the excitation period (subharmonic). As an example, a 1/2 subharmonic attractor has a period, which is twice the excitation period. A quasi-periodic attractor is a geometrically defined object (a torus) in the phase space that, when viewed in the time domain, appears to be composed of a non-linear combination of two or more periodic signals with incommensurate frequencies. A chaotic attractor is characterized by a broad band spectrum and by an extreme sensitivity for initial conditions.

Generally, nth *subharmonic* solutions occur near excitation frequency $n \times f$ if at excitation frequency f a resonance of the system exists. Then, in the nth subharmonic solutions the frequency f appears. For instance, if a resonance frequency in a system exists at 20 Hz, generally a 1/2 subharmonic solution exists near $2 * 20 = 40$ Hz, while a 1/3 subharmonic solution exists near $3 * 20 = 60$ Hz, etc. An nth *superharmonic* resonance peak generally can be found at $1/n \times f$. In that resonance peak again the resonance frequency f appears. For example, if at 20 Hz a resonance of the system exists, a 2nd superharmonic resonance peak can be found near $20/2 = 10$ Hz, while a 3rd superharmonic resonance peak can be found at $20/3 = 6{\cdot}7$ Hz, etc. This means that if the resonance frequencies of a system are known, one can easily predict the location of the superharmonic and subharmonic resonances of the system. Of course, the existence of the superharmonic and subharmonic resonances depends on the damping level and the type of non-linearities in the system.

Most of the recent research concerning impact oscillators is based on single-degree-of-freedom models. (An overview can be found in Bishop [5].) Single-degree-of-freedom models capture important first-order information about a lot of the non-linear phenomena in the low-frequency range, in particular the location of the most important resonance zones. In Van de Vorst *et al*. [6] the need of adding more degrees of freedom (d.o.f.) (higher eigenmodes) for an accurate low frequency response is investigated by analysing a periodically driven beam system with an elastic stop at its middle. They concluded that the eigenmodes corresponding to high eigenfrequencies can have a large influence on the low frequency steady state response. In comparison to the response of a single-d.o.f. system, the higher eigenmodes cause extra (superharmonic) resonance peaks and disappearance of subharmonic solutions.

The objective of this paper is to investigate experimentally the influence of higher eigenmodes on the low frequency system response of a system with an elastic stop. Furthermore it is investigated whether an elastic stop can be modelled using the contact force law of Hertz [7, 8]. The verification is mainly focused on comparing periodic responses. Experiments are carried out using a clamped steel beam with a spherical aluminum contact hitting a second aluminum contact if the relative displacement at the contact point is negative. The whole system is base excited by a moving support.

As mentioned earlier, in the numerical analysis the elastic stop is modelled using Hertz's contact force law. Hence, the collision forces act in a continuous way. The beam system can be divided into a linear and a non-linear component. The linear component (the beam) is modelled by means of the finite element method and consequently has many more d.o.f. than the non-linear one. Because the numerical analysis of the resulting non-linear system is very expensive from a computational point of view, in particular for increasing number of d.o.f., it is worthwhile to keep the number of d.o.f. as low as possible. This can be achieved by applying a reduction method to the finite element model of the linear component. The particular reduction method applied is the component mode synthesis

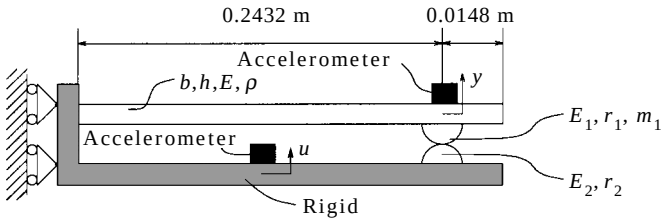

Fig. 1. Experimental set-up of beam system: $b = 0{\cdot}0298$ m, $h = 0{\cdot}0020$ m, $E = 2{\cdot}1 \times$ E11 N/m^2, $p = 7800$ kg/m^3.

method [9, 10] and offers the possibility for a considerable reduction of the d.o.f. Moreover, the component mode synthesis method can easily be used for geometrically more complex linear components. The component mode synthesis method used in this paper is based upon free-interface eigenmodes up to a cut-off frequency and residual flexibility modes to approximate the dynamic behaviour of the linear component. After reduction of the linear component the non-linear elements are added, resulting in a reduced non-linear system which will be valid for frequencies up to the cut-off frequency used in the reduction procedure. Because generically in non-linear responses higher frequencies than the excitation frequency are present, the cut-off frequency has to be chosen much higher than the maximum excitation frequency. Periodic solutions of the reduced system are calculated while varying the excitation frequency by solving two-point boundary value problems using the multiple shooting method [11] in combination with a path-following method [10].

In section 2 the experimental set-up of the beam system is given. In section 3 the steady state behaviour of the beam system is investigated numerically by calculating periodic solutions. In section 4 the experimental results for the beam system are compared with the numerical results. Finally, in section 5 some conclusions are drawn.

2. BEAM SYSTEM WITH AN ELASTIC STOP

Figure 1 shows the beam system which is analysed both numerically and experimentally. The beam is clamped on one side to a vibrating table and has a spherical elastic contact on the other side. If the relative displacement $(y - u)$ of the right-hand side of the beam is negative, it hits another spherical elastic contact which is also connected to the vibrating table. Using the vibrating table, which is driven by an electric motor, this spherical contact

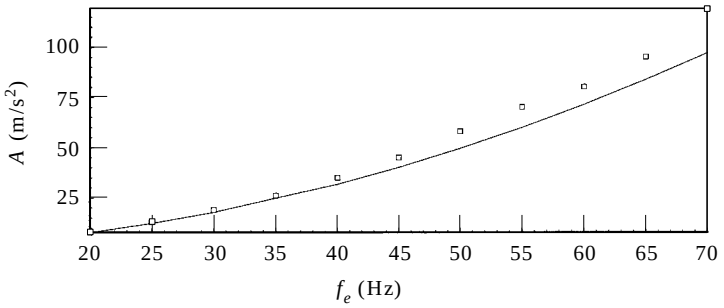

Fig. 2. Calculated and measured amplitudes of prescribed acceleration of vibrating table for varying excitation frequency f_e, ——, calculated amplitude acceleration, □, measured amplitude acceleration.

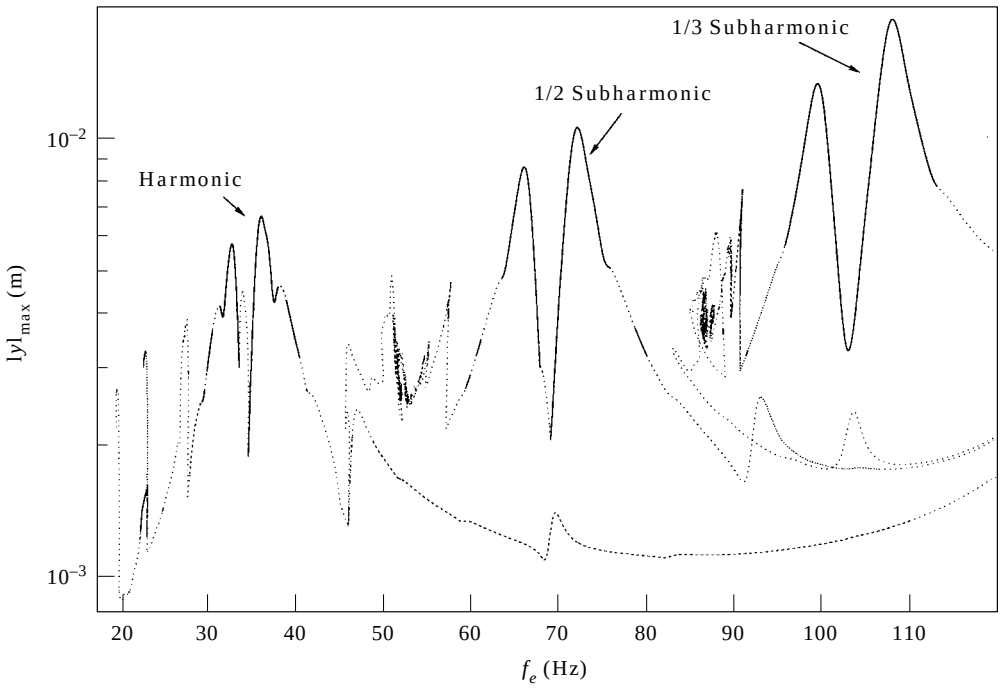

Fig. 3. Maximum displacements of periodic solutions of a six-d.o.f. model with $\xi_m = 0{\cdot}015$: -----, unstable; ——, stable.

and the left-hand side of the beam are base excited with a prescribed vertical displacement $u(t) = 0{\cdot}5015 \cos(2\pi f_e t)$ mm.

As mentioned in section 1, in the numerical analysis the system is divided into two components: a linear component (the linear beam with periodically driven frictionless sliding support in the y-direction on the left-hand side) and a non-linear component (the elastic contact). The linear component is modelled using finite elements and subsequently reduced. In the reduction two residual flexibility modes (one for the left end base excitation and one for the elastic stop), one rigid body mode and four free-interface eigenmodes ($f_1 = 30{\cdot}51$ Hz, $f_2 = 192{\cdot}68$ Hz, $f_3 = 507{\cdot}26$ Hz and $f_4 = 973{\cdot}45$ Hz) are included. This results in a six-d.o.f. model for the *reduced* clamped beam with eigenfrequencies: $f_1 = 17{\cdot}495$ Hz, $f_2 = 137{\cdot}28$ Hz, $f_3 = 414{\cdot}33$ Hz, $f_4 = 843{\cdot}26$ Hz, $f_5 = 1538{\cdot}8$ Hz and $f_6 = 3940{\cdot}9$ Hz. The first six eigenfrequencies of the *unreduced* clamped linear beam are $f_1 = 17{\cdot}495$ Hz, $f_2 = 137{\cdot}28$ Hz, $f_3 = 414{\cdot}33$ Hz, $f_4 = 842{\cdot}91$ Hz, $f_5 = 1419{\cdot}7$ Hz and $f_6 = 2136{\cdot}1$ Hz, so the last three eigenfrequencies of the reduced system are 0·04, 8 and 84% inaccurate, respectively, and the reduced model is accurate up to approximately 1000 Hz. Compared to the maximum excitation frequency of 70 Hz this is very high. However, because of the elastic stop, the frequencies generated by the system will be much higher than the maximum excitation frequency.

As mentioned in section 1, the contact force F_s between two equal spherical elastic contacts is modelled using Hertz's law [7, 8], that is

$$F_s(y, u) = \begin{cases} k_s(y-u)^{3/2}, & (y-u) \geqslant 0 \\ 0, & (y-u) < 0 \end{cases}. \tag{1}$$

In equation (1) the parameter k_s is taken as $4{\cdot}5 \times 10^9\ \mathrm{Nm}^{2/3}$ for contact radii $r_1 = r_2 = 15$ mm and Young's moduli $E_1 = E_2 = 7{\cdot}0 \times 10^{10}\ \mathrm{N/m}^2$ of the aluminum spherical contacts. The mass of the spherical contact (including the accelerometer) is $m_1 = 37{\cdot}56$ g.

The damping in the system without elastic contact is estimated experimentally using logarithmic decrement evaluation. According to this estimation, the damping in the model can be taken into account by adding modal damping with a modal damping coefficient of $\xi_m = 0{\cdot}003$ for each eigenmode. Calculations using this damping level showed in some frequency ranges such a complex path with periodic solutions that a very large number of periodic solutions has to be calculated to follow the path. Furthermore almost all calculated periodic solutions appeared to be unstable. In the real system, damping also is present during the impact time. This is not modelled in the numerical analysis. Because of this, branches of periodic solutions have also been calculated using a modal damping coefficient of $\xi_m = 0{\cdot}015$. Using this modal damping coefficient, all the branches can be followed with a limited number of periodic solutions.

In the experiments two accelerometers are used. One is placed at the position of the elastic contact on the beam measuring $\ddot{y}$. The other one is placed at the vibrating table measuring $\ddot{u}$. The choice to measure accelerations instead of displacements or velocities is due to the fact that it is simple to measure accelerations in a broad frequency band at the tip of the beam by means of an accelerometer. It would have been possible, at least in principle, to measure displacements with linear variable differential transformers (LVDT's). However, the LVDT's available in the authors' laboratory are accurate only up to $+/-0{\cdot}6$ cm, whereas during the experiments the displacements mounted up to 4 cm in one direction. It would also be possible to measure displacements with laser-interferrometry. This complicates the measurements considerably and also makes them very expensive.

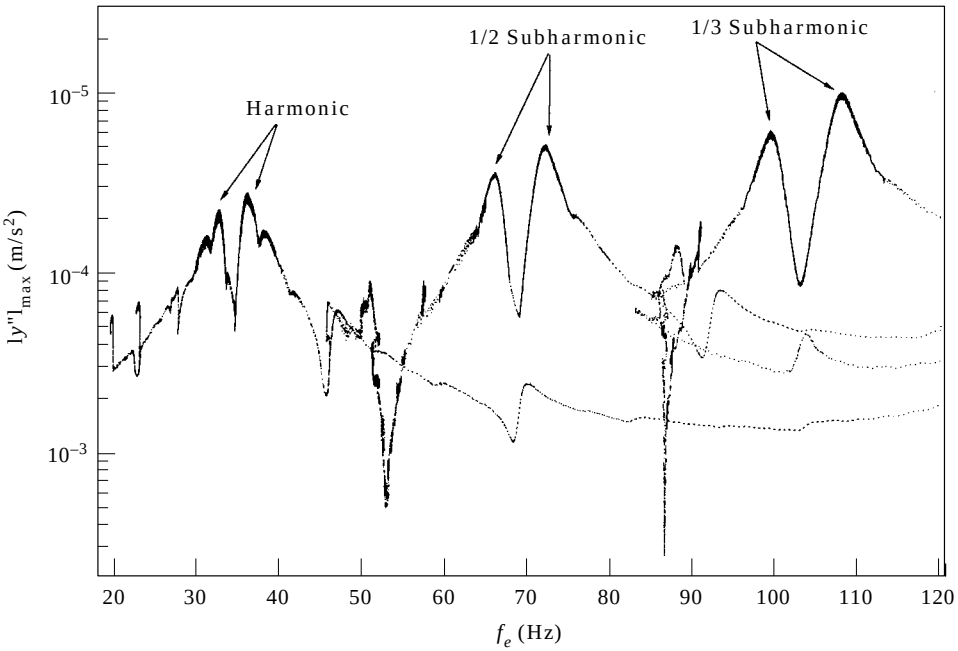

Fig. 4. Maximum accelerations of periodic solutions of a six-d.o.f. model with $\xi_m = 0{\cdot}015$; -----, unstable; ——, stable.

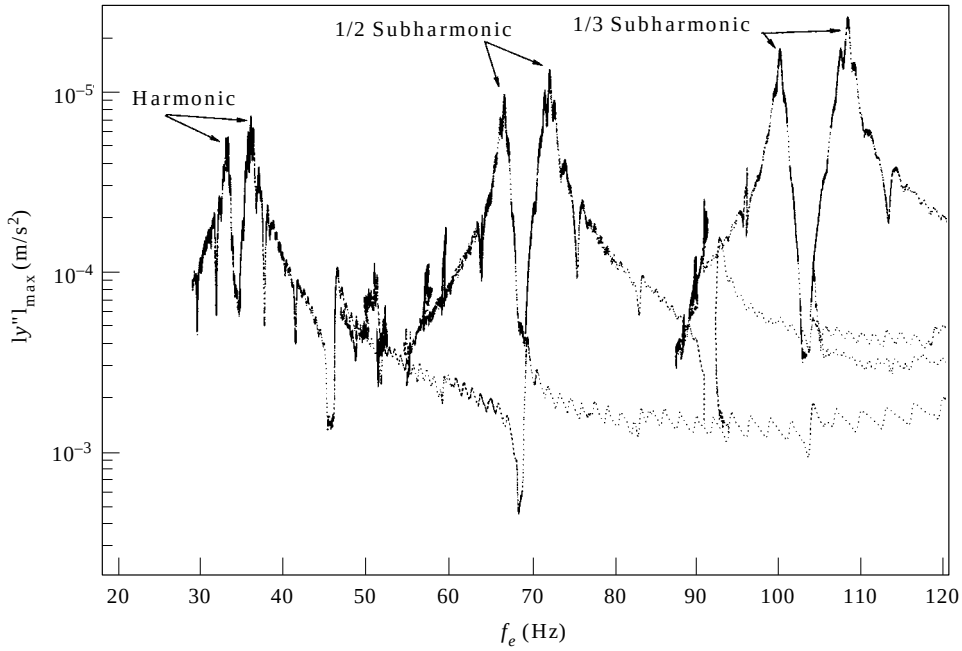

Fig. 5. Maximum accelerations of periodic solutions of a six-d.o.f. model with $\xi_m = 0{\cdot}003$; -----, unstable; ——, stable.

Because of the limited power of the electric motor, the maximum excitation frequency which can be used in the experiment is 70 Hz. Acceleration measurements showed that the prescribed displacement is practically sinusoidal between 20 and 70 Hz. For frequencies lower than 20 Hz, high frequencies occur on top of the sinusoidal signal due to the eigenfrequencies of the driving mechanism. As mentioned in section 2, the amplitude of the prescribed displacement of the vibrating table is 0·5015 mm. Figure 2 shows the amplitudes of the measured and numerical accelerations ($0{\cdot}5015(2\pi f_e)^2$) of the vibrating table for varying excitation frequency. The results in the figure indicate that the difference between calculated and measured amplitudes increases for increasing excitation frequency to about 23% for $f_e = 70$ Hz. This is due to the mass of the vibrating table and the flexibility of the drive. Numerical simulations showed that the amplitude of the acceleration does not strongly influence the qualitative behaviour of the system.

In the acceleration measurements of $\ddot{y}$ many high frequencies are present due to the low damping in the system. In order to be able to assess the measured accelerations, the measurement data is filtered by a low pass filter with a bandwidth of 850 Hz.

The elastic contacts did not show any plastic deformation after the experiments. This is important because plastic deformation will result in a change of the contact radius of the spherical contacts and hence also in a change of the Hertzian constant. It was observed that the surface at the area of elastic contacts became black after carrying out some experiments probably due to oxidation of the aluminum. The measurements in the frequency range 20–70 Hz were carried out twice. In both measurements, the same results were obtained and this also indicates the absence of plastic deformation in the contact area and also that the oxidation of the aluminum does not affect the experimental results.

3. NUMERICAL ANALYSIS

Figure 3 shows the maximum absolute displacements y (the position of the elastic contact on the beam) occurring in the calculated periodic solutions for varying excitation frequency f_e for $\xi_m = 0{\cdot}015$. The results depicted in Figure 3 have been obtained from 42 000 computed periodic solutions.

Figure 3 shows a harmonic branch with periodic solutions and also a 1/2 and a 1/3 subharmonic branch with periodic solutions. Near 34 Hz two harmonic resonance peaks occur on the harmonic branch. These two harmonic resonance peaks are related to the first eigenmode of the linear system ($f_1 = 17{\cdot}495$ Hz) and the second eigenmode of the linear system ($f_2 = 137{\cdot}28$ Hz). Due to the very stiff elastic contact, the stiffness of the system as a whole increases and the first resonance frequency shifts from 17 Hz in the linear system to approximately 34 Hz in the non-linear system. The fourth superharmonic resonance peak of the second resonance frequency of the system is located near this resonance frequency because $f_4/4 = 137{\cdot}28/4 \approx 34$ Hz. In the periodic solutions indeed in this frequency range the frequency of 137 Hz becomes more dominant. Apparently, the fourth superharmonic resonance causes an anti-resonance which splits the first harmonic resonance peak into two peaks.

Furthermore, on the harmonic branch superharmonic resonance peaks occur. Figure 3 shows a second (near 70 Hz), a third (near 47 Hz), a fifth (near 29 Hz), a sixth (near 24 Hz) and a seventh (near 20 Hz) superharmonic resonance peak related to the second resonance frequency ($f_2 \approx 137$ Hz) of the system. The superharmonic resonance peaks related to the third resonance frequency ($f_3 \approx 414$ Hz) of the system are much smaller but can still be

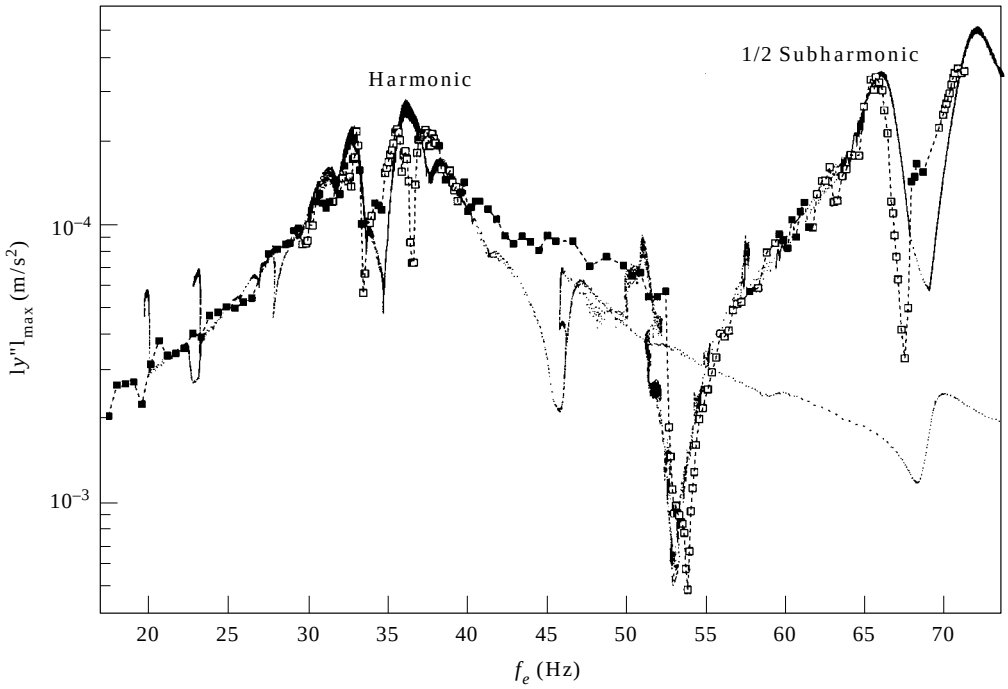

Fig. 6. Numerical and shifted experimental maximum accelerations of periodic solutions of a six-d.o.f. model with $\xi_m = 0{\cdot}015$; -----, numerical (unstable); ——, numerical (stable); □, experimental (periodic); ■, experimental (aperiodic).

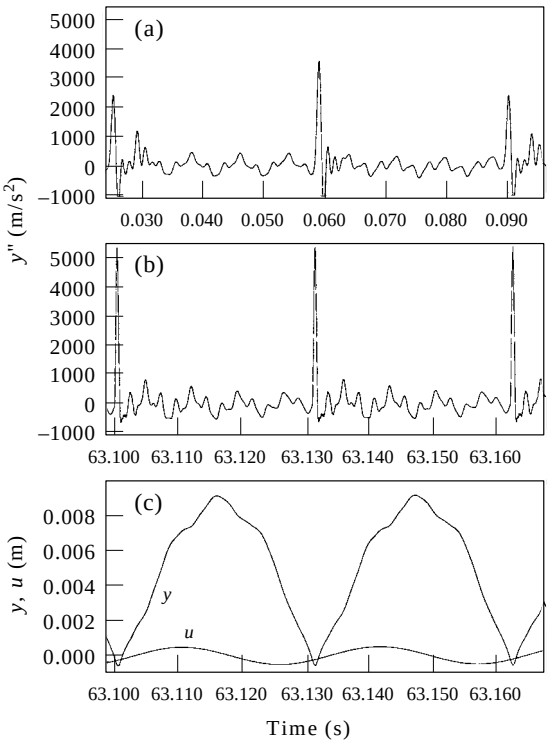

Fig. 7. (a) Experimental ($f_e = 31{\cdot}0$ Hz) and (b,c) numerical ($f_e = 32{\cdot}34$ Hz) harmonic signals.

seen on the harmonic branch in Figure 3 (for instance the tenth superharmonic resonance peak occurs near 41 Hz).

The 1/2 subharmonic and 1/3 subharmonic branches shown in Figure 3 are related to the first resonance frequency of the system. Notice that they are higher than the first resonance peak. This is due to the increasing amplitude of the prescribed acceleration for higher frequencies. Just like the first resonance peak on the harmonic branch, the resonance peaks on the 1/2 subharmonic branch and 1/3 subharmonic branch are split into two peaks. It seems that the harmonic branch is projected on the 1/2 subharmonic and 1/3 subharmonic branches. Near 93 Hz on the 1/2 subharmonic branch a superharmonic resonance peak occurs which is related to the third superharmonic resonance peak related to the second resonance frequency of the system on the harmonic branch.

In the frequency ranges 41–65 and 78–95 Hz only a few stable periodic solutions were found. In these frequency ranges mainly chaotic behaviour was found. Also between the highest resonance peaks on the harmonic and 1/2 subharmonic branches chaotic behaviour was found.

Figures 4 and 5 show the maximum absolute accelerations $|\ddot{y}|_{\max}$ of the beam at the elastic contact occurring in the periodic solutions for varying excitation frequency for the model with $\xi_m = 0{\cdot}015$ and $\xi_m = 0{\cdot}003$. A part of the 1/2 subharmonic branch of the model with $\xi_m = 0{\cdot}003$ was not calculated near 53 Hz due to the complexity of the branch (see also earlier discussion in section 2). For the same reason a part of the (unstable) 1/3 subharmonic branch was not calculated in the frequency range 85–104 Hz. For determining the response of the system with $\xi_m = 0{\cdot}003$, 71 000 periodic solutions were calculated.

Figure 5 indicates that the model with $\xi_m = 0{\cdot}003$ shows much more superharmonic resonance peaks related to high resonance frequencies on the harmonic branch. Due to the low modal damping of these resonance frequencies, the corresponding eigenmodes are more strongly excited. Furthermore, the model with $\xi_m = 0{\cdot}003$ shows higher harmonic, 1/2 subharmonic and 1/3 subharmonic resonance peaks in comparison to the model with $\xi_m = 0{\cdot}015$. Also more superharmonic resonance peaks occur on top of these resonance peaks in the case $\xi_m = 0{\cdot}003$. Calculations using a model reduced to eight d.o.f. instead of six and $\xi_m = 0{\cdot}003$ showed that adding more d.o.f. results in more (small) superharmonic resonance peaks on top of the harmonic, 1/2 subharmonic and 1/3 subharmonic resonance peaks. Apparently numerous eigenmodes are excited near these resonance peaks. Apart from the resonance peaks, the branches of the models with $\xi_m = 0{\cdot}003$ and $0{\cdot}015$ have the same maximum acceleration level. Notice that near 53 Hz the maximum acceleration of the model with $\xi_m = 0{\cdot}015$ is very low. This is described in more detail in the next section.

4. EXPERIMENTAL ANALYSIS

Measurements using the linear beam system without elastic contact showed that the first three eigenfrequencies of the linear beam are 17·2, 128·9 and 378·9 Hz which are approximately 2, 6 and 9% lower than the calculated eigenfrequencies $f_1 = 17{\cdot}495$ Hz, $f_2 = 137{\cdot}28$ Hz, $f_3 = 414{\cdot}33$ Hz. Apparently, the system parameter values in the experimental set-up (E, ρ, mass of elastic contact, etc.) differ from the system parameter values in the numerical model. Because of this the experimental results of the non-linear system are shifted to a lower frequency.

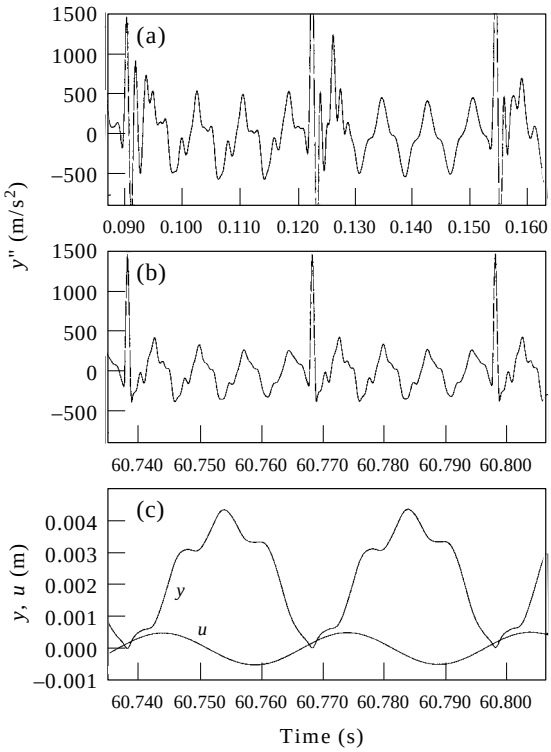

Fig. 8. (a) Experimental ($f_e = 31{\cdot}5$ Hz) and (b,c) numerical ($f_e = 33{\cdot}6$ Hz) harmonic signals.

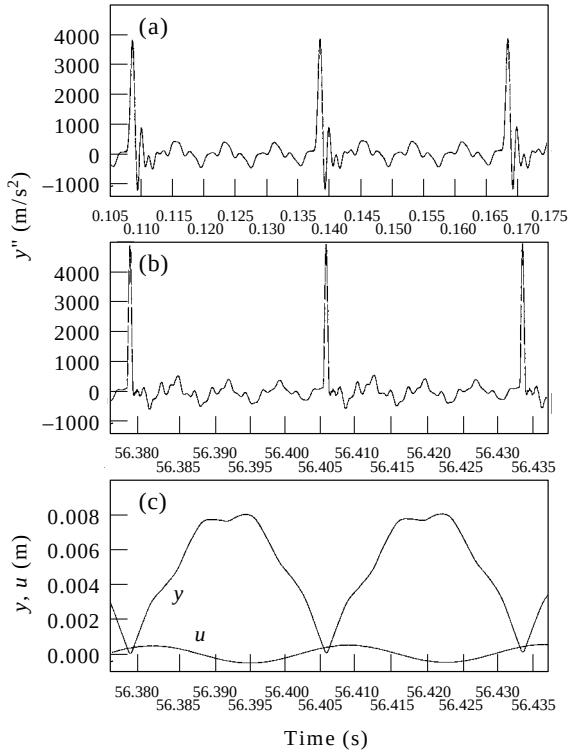

Fig. 9. (a) Experimental ($f_e = 33{\cdot}6$ Hz) and (b,c) numerical ($f_e = 36{\cdot}2$ Hz) harmonic signals.

As mentioned in section 2 the measured accelerations are filtered by a low pass filter with a bandwidth of 850 Hz. Some experiments were carried out without a low pass filter. The maximum accelerations obtained without a low pass filter showed a shift compared to the experimental results obtained using the filter. Without a low pass filter, the experimental maximum accelerations resemble the numerical maximum accelerations. Hence, the low pass filter causes a maximum acceleration shift. The highest accelerations occur at the moment when the beam hits the elastic contact. At that moment in a very small time interval the accelerations are much larger than the accelerations of the beam if it does not make contact with the elastic stop. Because of this, the low pass filter reduces the maximum accelerations.

Figure 6 shows the measured maximum absolute acceleration occurring in the signals for varying excitation frequency (symbols) together with the calculated branches for $\xi_m = 0{\cdot}015$ (lines). In order to compare the experimental and numerical results, the experimental maximum accelerations are shifted in the positive frequency direction 6% and are shifted in the positive maximum acceleration direction by 600%. Apart from a frequency shift and a maximum acceleration reduction, the experimental and numerical results for the beam system with elastic contact agree very well.

The measured accelerations are divided into two categories, namely periodic signals and aperiodic signals. As far as the aperiodic signals are concerned, in Figure 6 the maximum absolute accelerations are plotted. Note that because of this the experimental and numerical results cannot be compared entirely, since in the calculated response only periodic signals (stable and unstable) are used. Most of the aperiodic signals are chaotic signals. This can be checked by calculating Lyapunov exponents of these signals [12, 13].

This paper is focused on the measured periodic signals since these can be more easily compared to numerically obtained periodic signals.

In Figure 6 the experimental results agree very well with the numerical results. Just as in the numerical results, two harmonic resonance peaks occur near 34 Hz in the experiments. However, the right harmonic resonance peak has a dip in the experiment and this was not found in the numerical results. Due to the limited power of the electric motor, it could not be investigated whether the right 1/2 subharmonic resonance peak on the 1/2 subharmonic branch also has a dip. As mentioned in the previous section, all peaks on top of the harmonic resonance peaks are projected to the 1/2 subharmonic resonance peaks. In the numerical response a dip exists for $f_e = 37{\cdot}65$ Hz. However, this dip does not exist on top of the right harmonic resonance peak as in the experimental results.

In Figures 7–10 some experimental and numerical periodic signals are shown which occur near the first harmonic resonance peak. In the figures the measured and numerical contact point acceleration, the numerical contact displacement and the prescribed foundation displacement are shown. Because of the earlier mentioned frequency shift between the numerical and experimental results, the periodic signals are compared for different frequencies for which the signals show the best agreement. The measured accelerations which are shown in the figures, are filtered by the earlier mentioned low pass filter with a bandwidth of 850 Hz. In Figures 7–9 the experimental and numerical results agree well. Notice that in the figures the maximum acceleration in the numerical signals is lower than can be expected from Figure 6 (Figure 6 gives the maximum absolute accelerations occurring in the signals). This is caused by the fact that the maximum

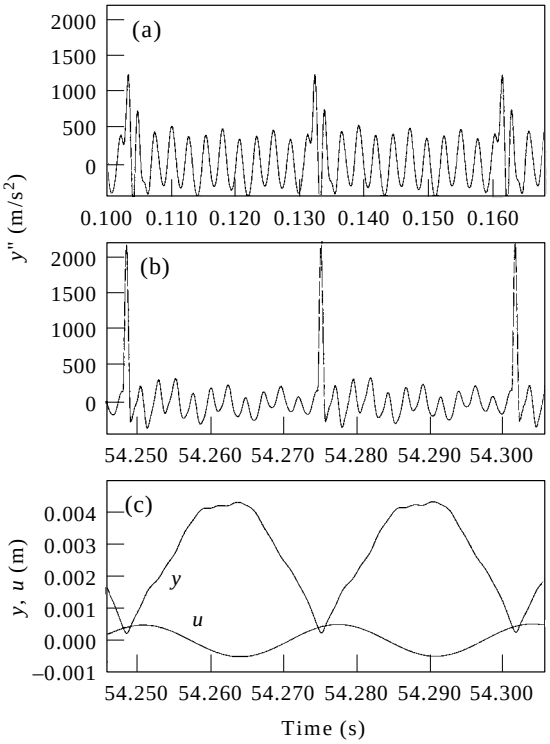

Fig. 10. (a) Experimental ($f_e = 34{\cdot}5$ Hz) and (b,c) numerical ($f_e = 37{\cdot}64$ Hz) harmonic signals.

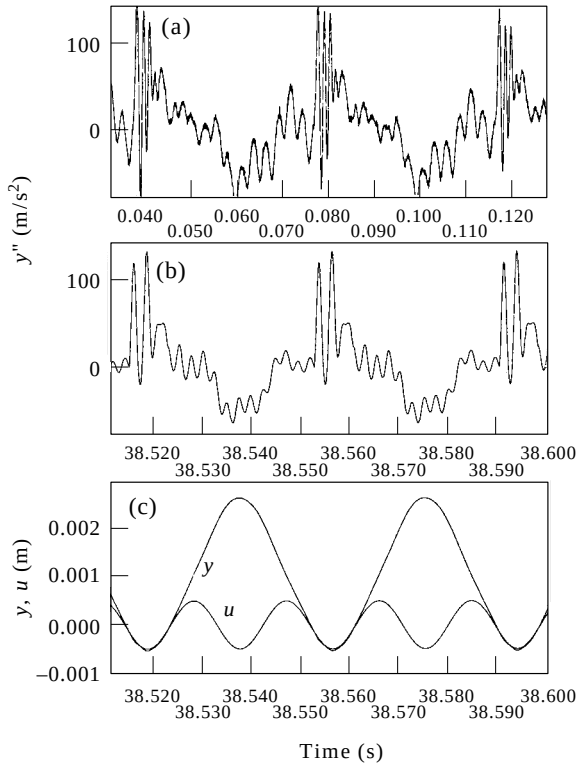

Fig. 11. (a) Experimental ($f_e = 50{\cdot}8$ Hz) and (b,c) numerical ($f_e = 53{\cdot}0$ Hz) 1/2 subharmonic signals.

acceleration occurs in a very small time interval and because of time discretization in Figures 7–9, the maximum acceleration occurring in the plotted calculated signals is lower.

In Figure 10 the experimental and numerical acceleration signals are compared for $f_e = 34{\cdot}5$ and $37{\cdot}64$ Hz, respectively. At $f_e = 34{\cdot}5$ Hz the experimental results show a dip (Figure 6) in the right first harmonic resonance peak. As mentioned earlier, in the numerical results a dip exists for $f_e = 37{\cdot}64$ Hz, for which the value is 2 Hz higher than expected if the experimental results have a 6% frequency shift. Figure 10 shows that apart from the largest acceleration, the experimental and numerical signals agree well. The acceleration dip in the numerical results is related to the eleventh superharmonic resonance peak of the third resonance frequency of the non-linear system ($11 \times 37{\cdot}64 = 414$ Hz $\approx f_3$). Apparently, the third eigenfrequency in the experiment is about $11 \times 34{\cdot}5 = 379{\cdot}5$ Hz. As mentioned earlier the third eigenfrequency of the linear beam was experimentally determined to be $378{\cdot}9$ Hz, so this confirms that the acceleration dip is caused by the eleventh superharmonic of the third eigenfrequency. Because the third eigenfrequency of the numerical linear model differs approximately 9% from the eigenfrequency of the experimental linear beam, in the numerical analysis the dip related to the third eigenfrequency does not occur on top of the right harmonic resonance peak but at $f_e = 37{\cdot}64$ Hz.

Near $f_e = 53{\cdot}0$ Hz the maximum acceleration in both the numerical and experimental results is very low. Figure 11 shows the experimental and numerical periodic signals for $f_e = 50{\cdot}8$ and 53 Hz, respectively. Both signals agree very well and the numerical time–displacement plot shows why the acceleration is so small in this frequency range: if the elastic stop hits the beam, both the elastic stop and beam have approximately the same

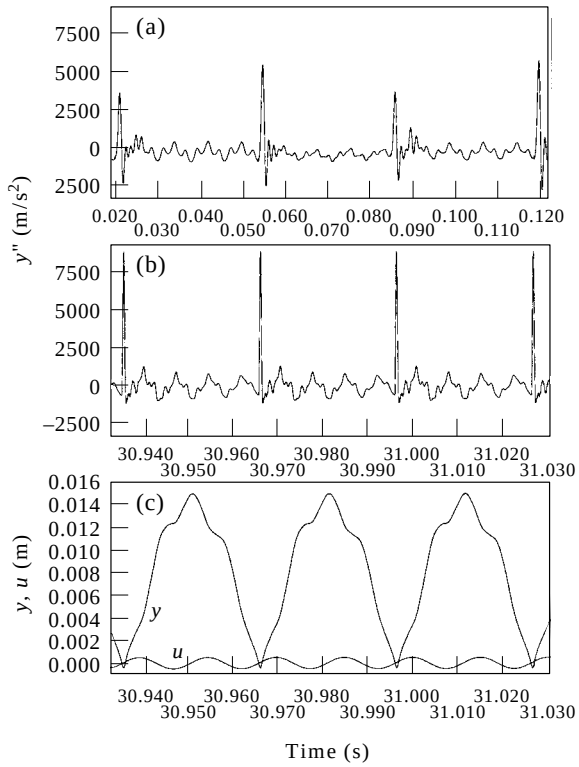

Fig. 12. (a) Experimental ($f_e = 61{\cdot}65$ Hz) and (b,c) numerical ($f_e = 61{\cdot}65$ Hz) 1/2 subharmonic signals.

velocity and this holds for the entire contact time. In the experiment, for this frequency range the noise produced by the experimental set-up was surprisingly low.

In Figures 12–14 some experimental and numerical periodic signals are shown which occur near the 1/2 subharmonic resonance peak. Again the experimental and numerical results agree very well. Notice that for $f_e = 67{\cdot}8$ Hz also a considerable high frequency component is present in the time–displacement plot. This high frequency component f_h has four periods per two excitation periods: $f_h = (67{\cdot}8/2) \times 4 = 135{\cdot}6$ Hz $\approx f_2 = 137{\cdot}28$ Hz. This confirms that the dip between the two harmonic and 1/2 subharmonic resonance peaks is related to the fourth superharmonic resonance peak of the second resonance frequency of the system. Notice also the similarity of the periodic solutions near the first harmonic resonance peak (Figures 7–9) and the 1/2 subharmonic resonance peak (Figures 12–14).

5. CONCLUSIONS

In this paper, a periodically driven beam system with an elastic contact was investigated both experimentally and numerically. Apart from a frequency shift and a maximum acceleration reduction, the experimental and numerical results agree very well. The results indicate that higher eigenmodes of the beam play an important role in the low frequency response of the system. Especially near the harmonic and 1/2 subharmonic resonance peaks, many high frequency eigenmodes are excited. The experimental results indicate that the elastic contact can be modelled using the contact force law of Hertz.

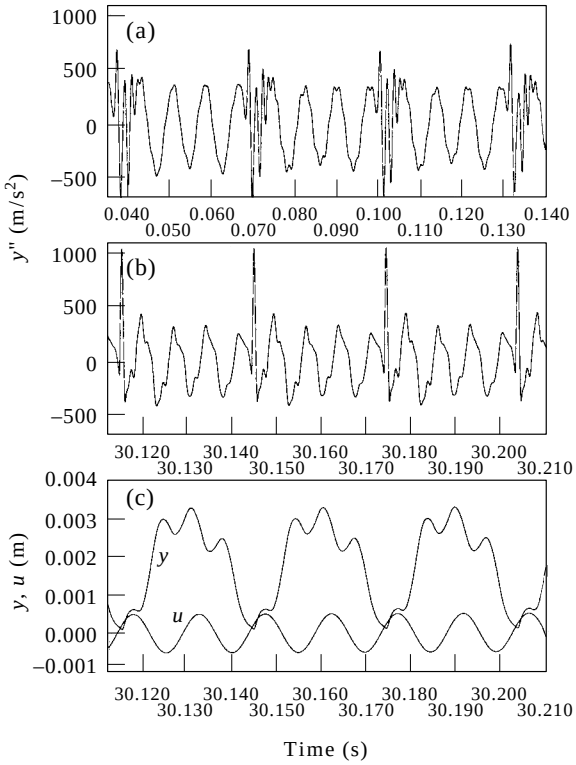

Fig. 13. (a) Experimental ($f_e = 63{\cdot}7$ Hz) and (b,c) numerical ($f_e = 67{\cdot}8$ Hz) 1/2 subharmonic signals.

The damping in the *linear* system was experimentally determined to be approximately $\xi_m = 0{\cdot}003$. However, section 4 shows that the results obtained using a modal damping coefficient of $\xi_m = 0{\cdot}015$ correspond much better. Apparently, the dissipation in the *non-linear* system is much higher due to the elastic contact. This energy dissipation was not modelled in the numerical model. One has to take into account that by increasing the modal damping coefficient, the damping of all eigenmodes is increased. In the actual system, the energy dissipation caused by the elastic contact is concentrated on one position of the beam (at the contact area). At this point the numerical model can be improved by using a hysterestic damping model in Hertz's law, for instance the model of Lankarani and Nikravesh [14].

In the experiments a low pass filter was used in order to get a better comparison between experimental and numerical results. A disadvantage of this filter is that the maximum accelerations which occur in the measured signals are reduced considerably. As mentioned before, near the resonance peaks, the numerical model which is valid up to 1000 Hz is not accurate enough for approximating the actual system. For these frequency ranges, a filter bandwidth of above 1000 Hz should be used instead of the filter bandwidth of 850 Hz used in this paper. Also it would be preferable to measure displacements instead of accelerations in future experiments, since displacement signals do not show as many high frequencies as acceleration measurements. Because of this, the experimental and numerical displacement signals can be compared more easily, probably even without using a low pass filter.

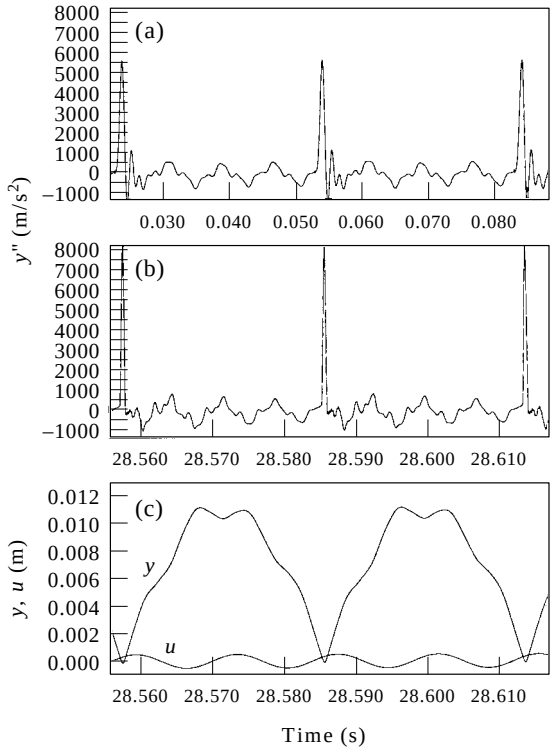

Fig. 14. (a) Experimental ($f_e = 66{\cdot}5$ Hz) and (b,c) numerical ($f_e = 71{\cdot}5$ Hz) 1/2 subharmonic signals.

ACKNOWLEDGMENTS

This work was supported by the Centre for Mechanical Engineering of TNO Building and Construction Research, Delft, The Netherlands. All calculations presented in this paper were carried out using a development release of the finite element package DIANA [15]. The authors are much indebted to useful comments by the anonymous reviewers.

REFERENCES

1. J. Guckenheimer and P. Holmes 1983 *Nonlinear Oscillations, Dynamical Systems, and Bifurcations of Vector Fields*, Applied Mathematical Sciences, Vol. 42. Berlin: Springer.
2. J. M. T. Thompson and H. B. Stewart 1986 *Nonlinear Dynamics and Chaos*. New York.
3. T. S. Parker and L. O. Chua 1989 *Practical Numerical Algorithms for Chaotic Systems*. Berlin: Springer.
4. J. M. T. Thompson 1994 in *Nonlinearity and Chaos in Engineering Dynamics* (M. T. Thompson and S. R. Bishop, editors). Proceedings of the IUTAM Symposium, London. New York: Wiley. Basic concepts of nonlinear dynamics.
5. S. R. Bishop 1994 *Philosophical Transactions of the Royal Society of London* **347**, 345–448. Impact oscillators.
6. E. L. B. van de Vorst, D. H. van Campen, R. H. B. Fey and A. Kraker 1996 *Journal of Sound and Vibration* **192**, 913–925. Periodic solutions of a multi-dof beam system with impact.
7. H. Hertz 1895 *Gesammelte Werke, Vol.* 1: *Schriften vermischten inhalts*. Leipzig, Germany.
8. W. Goldsmith 1960 *Impact*: *The Theory and Physical Behaviour of Colliding Solids*. London: E. Arnold Ltd.

9. R. R. CRAIG JR. 1985 in *Combined Experimental/Analytical Modeling of Dynamic Structural Systems Using Substructure Synthesis* (D. R. Martinez and A. K. Miller, editors) 1–31. New York: ASME Applied Mechanics AMD-67. A review of time-domain and frequency-domain component mode synthesis methods.
10. R. H. B. FEY 1992 *PhD Thesis*, *Eindhoven University of Technology*, *Eindhoven*, *The Netherlands*. Steady-state behaviour of reduced dynamic systems with local non-linearities.
11. U. M. ASCHER, R. M. M. MATTHEIJ and R. D. RUSSELL 1988 *Numerical Solution of Boundary Value Problems for Ordinary Differential Equations*. Englewood Cliffs, NJ: Prentice-Hall.
12. A. WOLF, J. B. SWIFT, H. L. SWINNEY and J. A. VASTANO 1985 *Physica* **16D**, 285–317. Determining Lyapunov exponents from a time series.
13. E. L. B. VAN DE VORST, F. H. ASSINCK, A. DE KRAKER, R. H. B. FEY and D. H. VAN CAMPEN 1996 *Experimental Mechanics* **36**, 159–165. Experimental verification of the steady-state behaviour of a beam system with discontinuous support.
14. H. M. LANKARANI and P. E. NIKRAVESH 1994 *Nonlinear Dynamics* **5**, 193–207. Continuous contact force models for impact analysis in multibody systems.
15. *DIANA User's Manual*, 6.0 edition, 1996. Delft, The Netherlands: DIANA, TNO Building and Construction Research.